



HAL
open science

Stability of incompressible formulations enriched with X-FEM

Grégory Legrain, Nicolas Moes, Antonio Huerta

► **To cite this version:**

Grégory Legrain, Nicolas Moes, Antonio Huerta. Stability of incompressible formulations enriched with X-FEM. *Computer Methods in Applied Mechanics and Engineering*, 2008, 197 (21-24), pp.1835-1849. 10.1016/j.cma.2007.08.032 . hal-01007317

HAL Id: hal-01007317

<https://hal.science/hal-01007317>

Submitted on 9 Feb 2018

HAL is a multi-disciplinary open access archive for the deposit and dissemination of scientific research documents, whether they are published or not. The documents may come from teaching and research institutions in France or abroad, or from public or private research centers.

L'archive ouverte pluridisciplinaire **HAL**, est destinée au dépôt et à la diffusion de documents scientifiques de niveau recherche, publiés ou non, émanant des établissements d'enseignement et de recherche français ou étrangers, des laboratoires publics ou privés.

Stability of incompressible formulations enriched with X-FEM

G. Legrain^a, N. Moës^{a,*}, A. Huerta^b

^a *GeM Institute – École Centrale de Nantes/Université de Nantes/CNRS 1 Rue de la Noë, 44321 Nantes, France*

^b *Laboratori de Càlcul Numèric (LaCàN) – Edifici C2, Campus Nord, Universitat Politècnica de Catalunya – E-08034 Barcelona, Spain*

Received 18 July 2005; received in revised form 13 July 2007; accepted 13 August 2007

Available online 12 January 2008

Abstract

The treatment of (near-)incompressibility is a major concern for applications involving rubber-like materials, or when important plastic flows occurs as in forming processes. The use of mixed finite element methods is known to prevent the locking of the finite element approximation in the incompressible limit. However, it also introduces a critical condition for the stability of the formulation, called the inf-sup or LBB condition. Recently, the finite element method has evolved with the introduction of the partition of unity method. The eXtended Finite Element Method (X-FEM) uses the partition of unity method to remove the need to mesh physical surfaces or to re-mesh them as they evolve. The enrichment of the displacement field makes it possible to treat surfaces of discontinuity inside finite elements. In this paper, some strategies are proposed for the enrichment of low order mixed finite element approximations in the incompressible setting. The case of holes, material interfaces and cracks are considered. Numerical examples show that for well chosen enrichment strategies, the finite element convergence rate is preserved and the inf-sup condition is passed.

Keywords: Mixed formulation; X-FEM; Partition of unity; Inf-sup condition; Incompressibility; Holes; Inclusions; Fracture mechanics

1. Introduction

Displacement-based finite element methods are nowadays abundantly used in engineering analysis. Indeed, they can solve a wide variety of problems, and have now been deeply mathematically investigated. However, there still exists two main drawbacks for these methods. First, the treatment of incompressible or nearly incompressible problems necessitates the use of adapted formulations. If not, incompressibility constraint locks the approximation, leading for instance to non-physical displacement or pressure fields. Second, the generation and especially the update of the mesh in complex 3D settings for evolving boundaries such as cracks, material interfaces and voids still lacks robustness, and involves important human effort.

Several techniques have been developed to respond to the locking issue. For instance, the selective-reduced-inte-

gration procedures [1–3] or the Bbar approach of Hughes [4] in which the volumetric part of the strain tensor is evaluated at the center of the element. Another way to avoid locking is to enhance the strain tensor in order to enlarge the space on which the minimization is performed, and meet the divergence-free condition (enhanced assumed strain methods, see [5–9]).

Here, we will focus on low order two-field mixed finite element methods. The incompressibility constraint is weakened by the introduction of the pressure field. This alleviates locking at the price of additional pressure unknowns. However, mixed finite element methods are not stable in all cases, some of them showing spurious pressure oscillations if displacement and pressure spaces are not chosen carefully. To be stable, a mixed formulation must verify consistency, ellipticity and the so called inf-sup (or LBB) condition. The latter is a severe condition which depends on the connection between the displacement and pressure approximation spaces. Stable mixed formulations can be obtained by stabilizing non-stable formulations with the use of parameters whose values may depend on the

* Corresponding author.

E-mail addresses: gregory.legrain@ec-nantes.fr (G. Legrain), nicolas.moes@ec-nantes.fr (N. Moës), antonio.huerta@upc.edu (A. Huerta).

problem at hand. Otherwise, one has to work with approximation spaces which pass the inf–sup condition. To prove that a displacement–pressure pair satisfies the inf–sup condition is not a trivial task. However, a numerical test has been proposed by Brezzi and Fortin [10] and by Chapelle and Bathe [11], in order to draw a prediction on the fulfilment of the inf–sup. This test proved to be useful for the study of the stability of various mixed elements [12].

The second drawback of classical finite element methods (evolving boundaries) has been overcome by the development of alternative methods such as meshless methods in which the connectivity between the nodes is no longer obtained by the mesh, but by domains of influence which can be split by the boundaries. Moreover, the approximation basis can be enriched with functions coming from the a priori knowledge of the local character of the solution of the problem. Note that in the incompressible limit, meshless methods are now known to lock [13,14] as classical finite elements. Thus, some strategies have been developed to circumvent this issue [13,15]. Apart from mixing meshless methods and finite elements [16] another alternative to overcome the re-meshing issue in finite elements is to use partition of unity finite element methods which are based on the partition of unity concept introduced by Babuška and Melenk [17], and first employed in the context of the meshless method by Oden and Duarte [18,19]. Among the class of partition of unity finite element methods, the Generalized Finite Element Method (GFEM) and the eXtended Finite Element Method (X-FEM) are the most advanced. The GFEM was introduced by Strouboulis et al. [20–23] and was applied to the simulation of problems with complex micro-structures. The method was further extended to employ the idea of mesh-based numerically constructed handbook functions by Strouboulis et al. [24,25].

The X-FEM allows to model cracks, material inclusions and holes on non-conforming meshes, when used with proper enrichment of the finite element approximation. It has been applied to a wide variety of problems in fracture mechanics (2D [26–28], 3D [29–31], plates [32,33], cohesive zone modeling [34,35], dynamic fracture [36], non-linear fracture mechanics [37–39]), and in the study of heterogeneous media (holes [40,41], material inclusions [41,42] and multiple phase flows [43]).

Here, we focus on the application of this method to mixed formulations for the treatment of holes, material inclusions and cracks in the incompressible limit. Bbar or selective-reduced formulations are not considered, because they do not seem to generalize easily to enriched displacement fields. The main contribution of this paper is the design of enrichment strategies for the pressure and displacement fields, so that it leads to a stable formulation. The enrichment of mixed finite element approximations has already been used by Dolbow et al. [33] and Areias et al. [39] for fracture mechanics in plates and shells, and by Wagner et al. [44] for rigid particles in Stokes flow. However, the stability and the convergence of these approaches was not studied. The latest work concerning volumetric

incompressibility was proposed by Dolbow and Devan [37]. In this paper, the authors focus on the application of the enhanced assumed strain method to X-FEM in large strain. This approach seems to lead to a stable low order formulation in the case of nearly incompressible non-linear fracture mechanics. However, the stability of the method was not shown, and the influence of the near-tip enrichment was not studied. More precisely, it is not clear whether the near-tip enrichment could make this approach unstable, as the construction of an orthogonal enhanced strain field becomes difficult with non-polynomial functions.

The paper is organized as follows: first, the governing equations of incompressible linear elasticity are recalled. The conditions for the stability of mixed formulations are also reviewed. Next, some strategies are proposed to keep the stability of enriched finite elements. The case of holes, material interfaces and 2D cracks are presented. Finally, in a last section the stability of these strategies is investigated.

2. Governing equations

In this section, we focus on the design of stable mixed formulations for the treatment of incompressible elasticity under the assumption of small strain and displacement. First, the equations governing incompressible linear elasticity are recalled. Then the inf–sup condition is presented together with a numerical test.

2.1. Incompressible elasticity

We consider the static response of an elastic body (see Fig. 1) which occupies a bounded domain $\Omega \in \mathbb{R}^2$ with a sufficiently smooth boundary $\partial\Omega$ which is split into two disjoint parts: $\partial\Omega_u$ where displacements are prescribed (Dirichlet boundary conditions) and $\partial\Omega_T$ where tractions are prescribed (Neumann boundary conditions). The body is initially in an undeformed, unstressed state. The governing equations are

$$\begin{cases} \operatorname{div} \underline{\underline{\sigma}} + \mathbf{b} = \mathbf{0} & \text{on } \Omega, \\ \underline{\underline{\varepsilon}} = \frac{1}{2}(\nabla \mathbf{u} + \nabla \mathbf{u}^T) & \text{on } \Omega, \\ \underline{\underline{\sigma}} \cdot \mathbf{n} = \mathbf{T}_d & \text{on } \partial\Omega_T, \\ \mathbf{u}(\mathbf{x}) = \mathbf{u}_d & \text{on } \partial\Omega_u, \\ \underline{\underline{\sigma}} = \underline{\underline{\mathcal{C}}} : \underline{\underline{\varepsilon}} & \text{on } \Omega, \end{cases} \quad (1)$$

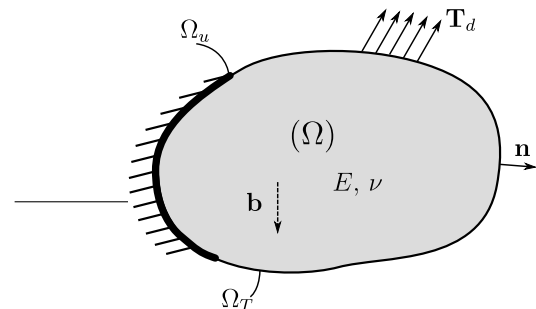


Fig. 1. The model problem.

where $\underline{\underline{\sigma}}$ is the Cauchy stress tensor, \mathbf{b} is the load per unit volume, \mathbf{u}_d is the prescribed displacement field, \mathbf{T}_d are the prescribed tractions, \mathbf{n} is the outward unit normal to the boundary $\partial\Omega$, $\underline{\underline{\varepsilon}}$ is the linearized strain tensor and $\underline{\underline{\mathcal{C}}}$ is the fourth order elasticity tensor which must be bounded, i.e. $\underline{\underline{\mathcal{C}}}_{ijkl} \in L^\infty(\Omega)$ $i, j, k, l = 1, 2, 3$. (2)

In the case of a linear isotropic elastic material, the constitutive equation can be written as

$$\underline{\underline{\sigma}} = \kappa \underline{\underline{\varepsilon}}_V(\mathbf{u}) \underline{\underline{I}} + 2\mu \underline{\underline{\varepsilon}}^D(\mathbf{u}) \text{ in } \Omega, \quad (3)$$

where ε_V is the volumetric strain ($\varepsilon_V(\mathbf{u}) = \text{div } \mathbf{u}$), κ is the bulk modulus,

$$\kappa = \frac{E}{3(1-2\nu)} \quad (4)$$

and $\underline{\underline{\varepsilon}}^D$ is the deviatoric strain operator:

$$\underline{\underline{\varepsilon}}^D = \underline{\underline{\varepsilon}} - \frac{\varepsilon_V}{3} \underline{\underline{I}}. \quad (5)$$

When the material tends to incompressibility, the bulk modulus tends to infinity. This means that ε_V must tend to zero (the displacement field must be divergence-free in the incompressible limit).

$$\varepsilon_V = \text{div}(\mathbf{u}) \rightarrow 0 \text{ as } \nu \rightarrow 0.5. \quad (6)$$

The strong form (1) is equivalent to the stationarity of a displacement potential Π :

$$\Pi(\mathbf{u}) = \frac{1}{2} \int_{\Omega} \underline{\underline{\varepsilon}}(\mathbf{u}) : \underline{\underline{\mathcal{C}}} : \underline{\underline{\varepsilon}}(\mathbf{u}) d\Omega - \int_{\Omega} \mathbf{u} \cdot \mathbf{b} d\Omega - \int_{\partial\Omega_T} \mathbf{u} \cdot \mathbf{T}_d d\Gamma. \quad (7)$$

In order to model incompressible or almost incompressible problems, a two field principle is considered by introducing a second variable (the hydrostatic pressure p) in the potential (7):

$$p = -\kappa \varepsilon_V(\mathbf{u}) = -\frac{1}{3} \text{Tr}(\underline{\underline{\sigma}}). \quad (8)$$

When κ increases, the volumetric strain ε_V decreases and becomes very small. For total incompressibility, the bulk modulus is infinite, the volumetric strain is zero, and the pressure remains finite (of the order of the applied boundary tractions). The stress tensor is then expressed as

$$\underline{\underline{\sigma}} = -p \underline{\underline{I}} + 2\mu \underline{\underline{\varepsilon}}^D \text{ in } \Omega. \quad (9)$$

The solution of the governing differential equations (1) now involves two variables: the displacement field and the pressure field. Writing the two fields variational principle, the total potential for the $u - p$ formulation is expressed as

$$\chi(\mathbf{u}, p) = \frac{1}{2} \int_{\Omega} \underline{\underline{\varepsilon}}^D(\mathbf{u}) : \underline{\underline{\mathcal{C}}} : \underline{\underline{\varepsilon}}^D(\mathbf{u}) d\Omega - \int_{\Omega} \mathbf{u} \cdot \mathbf{b} d\Omega - \int_{\partial\Omega_T} \mathbf{u} \cdot \mathbf{T}_d d\Gamma - \frac{1}{2} \int_{\Omega} \frac{p^2}{\kappa} d\Omega - \int_{\Omega} p \varepsilon_V(\mathbf{u}) d\Omega. \quad (10)$$

Invoking the stationarity of $\chi(\mathbf{u}, p)$ with respect to the two independent variables \mathbf{u} and p , we obtain

$$\int_{\Omega} \underline{\underline{\varepsilon}}^D(\delta\mathbf{v}) : \underline{\underline{\mathcal{C}}} : \underline{\underline{\varepsilon}}^D(\mathbf{u}) d\Omega - \int_{\Omega} p \varepsilon_V(\delta\mathbf{v}) d\Omega = R(\delta\mathbf{v}), \quad (11)$$

$$- \int_{\Omega} \left(\frac{p}{\kappa} + \varepsilon_V(\mathbf{u}) \right) \delta p d\Omega = 0, \quad (12)$$

where $R(\delta\mathbf{v})$ represents the virtual work of the external loads. In the case of two perfectly bounded materials (see Fig. 2), each phase of the body must satisfy (1) in addition to continuity conditions:

$$[[\mathbf{u}]] = \mathbf{0} \text{ on } \partial\Omega_2 \quad (13)$$

$$[[\underline{\underline{\sigma}}]] \cdot \mathbf{n}_2 = \mathbf{0} \text{ on } \partial\Omega_2, \quad (14)$$

where the jump operator $[[\cdot]]$ is defined along the interface, $\partial\Omega_2$, as $[[\mathbf{v}]] = \mathbf{v}_1 - \mathbf{v}_2$. Remark that (14) does not imply that the pressure is continuous across the interface.

2.2. Stability of mixed formulations

2.2.1. Analytical condition for stability – the inf-sup condition

The discretization of Eq. (11) leads to a finite element system in the form (see Section 3):

$$\begin{pmatrix} \mathbf{K}_{uu} & \mathbf{K}_{up} \\ \mathbf{K}_{up}^T & \frac{1}{\kappa} \mathbf{K}_{pp} \end{pmatrix} \begin{pmatrix} \mathbf{u} \\ p \end{pmatrix} = \begin{pmatrix} \mathbf{f} \\ \mathbf{0} \end{pmatrix} \quad (15)$$

In order to be regular in the full range of κ , the kernel of the \mathbf{K}_{up} matrix must be zero (as well of course as appropriate removal of the rigid modes).

More precisely, the displacement and pressure interpolations must satisfy the Ladyzhenskaya–Babuška–Brezzi compatibility condition [10], also known as the LBB (or inf-sup) condition. This condition states that the displacement and pressure spaces cannot be chosen separately. To ensure solvability, a necessary but not sufficient condition for the uniqueness of \mathbf{u} and p is that

$$\dim \mathcal{Q}^h \leq \dim \mathcal{V}^h, \quad (16)$$

where \mathcal{Q}^h and \mathcal{V}^h are respectively the pressure and displacement finite element spaces. The sufficient condition linking these spaces (inf-sup or LBB condition) expresses as

The existence of a stable finite element approximate solution (\mathbf{u}^h, p^h) depends on choosing a pair of spaces \mathcal{V}^h and \mathcal{Q}^h such that the following condition holds:

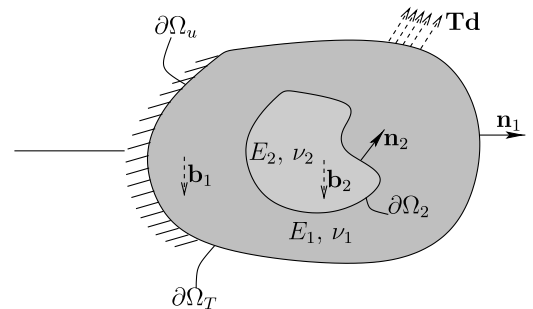


Fig. 2. The model problem with material interfaces.

$$\inf_{q^h \in \mathcal{Q}^h} \sup_{v^h \in \mathcal{V}^h} \frac{\int_{\Omega} q^h \operatorname{div} v^h d\Omega}{\|v^h\|_1 \|q^h\|_0} \geq \beta > 0, \quad (17)$$

where $\|\cdot\|_1$ and $\|\cdot\|_0$ indicates H^1 and L^2 norms, respectively, and β is independent of the mesh size h . If the inf-sup compatibility condition is satisfied, then there exists a unique $\mathbf{u}^h \in \mathcal{V}^h$ and a $p^h \in \mathcal{Q}^h$ (determined up to an arbitrary constant in the case of purely Dirichlet boundary conditions).

2.2.2. Numerical assessment of the inf-sup condition

As seen before, the prediction of the stability of a mixed formulation involves the fulfilment of the inf-sup criterion. This criterion is however impossible to prove for practical situations. This is why the numerical evaluation of the inf-sup condition has received considerable attention [11,10]. This numerical evaluation, although not equivalent to the analytical inf-sup, gives indications on whether (17) is fulfilled or not for a given set of finite element discretizations. The numerical inf-sup test is based on the following theorem.

Proposition 1. *Let $\mathbf{M}_{\mathbf{uu}}$ and $\mathbf{M}_{\mathbf{pp}}$ be the mass matrices associated to the scalar products of \mathcal{V}^h and \mathcal{Q}^h respectively and let μ_{\min} be the smallest non-zero eigenvalue defined by the following eigenproblem:*

$$\mathbf{K}_{\mathbf{up}}^T \mathbf{M}_{\mathbf{uu}}^{-1} \mathbf{K}_{\mathbf{up}} \mathbf{q} = \mu^2 \mathbf{M}_{\mathbf{pp}} \mathbf{q} \quad (18)$$

then the value of β is simply μ_{\min} .

The proof can be found in [45] or [10]. The numerical test proposed in [11] consists in testing a particular formulation by calculating β using meshes of increasing refinement. On the basis of three or four results it can be predicted whether the inf-sup value is probably bounded from underneath or, on the contrary, goes down to zero when the mesh is refined. The reliability of this test is demonstrated on several examples of elements for incompressible elasticity problems in [11]. In the following section this test is used to check the behavior of proposed enrichment strategies. However, we follow [11] and use only $\mathbf{S}_{\mathbf{uu}} = \int_{\Omega} \underline{\nabla} \mathbf{u} : \underline{\nabla} \mathbf{u} d\Omega$ instead of $\mathbf{M}_{\mathbf{uu}}$ in (18). In order to perform the numerical inf-sup test, a sequence of successive refined meshes is considered. The objective is to monitor the inf-sup values, β , when h decreases. If a steady decrease in $\log(\beta)$ is observed when h goes to zero, the element is predicted to violate the inf-sup condition and said to fail the numerical test. But, if the $\log(\beta)$ value is stable as the number of elements increases, the test is numerically passed.

3. X-FEM discretization

3.1. Displacement field

With classical finite elements, the approximation of a vector field \mathbf{u} on an element Ω_e is written as

$$\mathbf{u}(\mathbf{x})|_{\Omega_e} = \sum_{\alpha=1}^{n_u} u^{\alpha} \mathbf{N}_{\mathbf{u}}^{\alpha}(\mathbf{x}), \quad (19)$$

where n_u is the number of coefficients describing the approximation of the displacement over the element, u^{α} is the α th coefficient of this approximation and $\mathbf{N}_{\mathbf{u}}^{\alpha}$ is the vectorial shape function associated to the coefficient u^{α} . Within the partition of unity, the approximation is enriched as

$$\mathbf{u}(\mathbf{x})|_{\Omega_e} = \sum_{\alpha=1}^{n_u} \mathbf{N}_{\mathbf{u}}^{\alpha} \left(u^{\alpha} + \sum_{\beta=1}^{n_{\text{enr}}} a_{\beta}^{\alpha} \phi_{\beta}^u(\mathbf{x}) \right), \quad (20)$$

where n_{enr} is the number of enrichment modes, a_{β}^{α} is the additional dof associated to dof α and ϕ_{β}^u stands for the β th scalar enrichment function. The number and the expression of the enrichment functions vary with the problem to model. The expression of this enrichment function will be recalled for holes, inclusions and fracture mechanics in the next sections.

3.2. Pressure field

Using the same scheme, the pressure approximation is written as

$$p(\mathbf{x})|_{\Omega_e} = \sum_{\alpha=1}^{n_p} N_p^{\alpha} (p^{\alpha} + a^{\alpha} \phi^p(\mathbf{x})), \quad (21)$$

where n_p is the number of coefficients describing the approximation over the element, p^{α} is the α th coefficient of this approximation and N_p^{α} is the scalar shape function associated to the coefficient p^{α} , a^{α} is the additional dof associated to dof α and ϕ^p stands for the scalar pressure enrichment function. The key issue is the combined choice of enrichment functions ϕ^u and ϕ^p such that the whole enriched approximation (displacement and pressure) passes the inf-sup condition.

3.3. Stable mixed finite elements

In this work, we shall enrich two stable mixed finite elements: the Mini element introduced by Arnold et al. [46] and the *T6T3* which is a robust and classical mixed element (see Fig. 3). The Mini is composed of a linear displacement field plus a bubble function and linear pressure field (P_1^+, P_1 element), and the *T6T3* of a quadratic displacement field and a linear pressure field (P_2, P_1 element).

The theoretical convergence rates of these elements are, respectively, in $O(h)$ (for both pressure and displacement) for the Mini [46], and $O(h^2)$ (for both pressure and displacement) for the *T6T3* [47] in the corresponding norms.

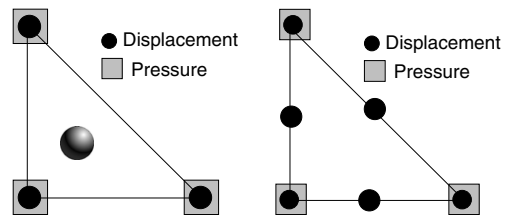


Fig. 3. The Mini element (left) and *T6T3* element (right).

4. Stability of mixed formulations enriched with X-FEM

4.1. The case of holes

The strategy for treating holes within the X-FEM consists in an integration of the weak form only in the non-void parts of the elements (see [40,41]). Moreover, the nodes for which the support is completely in the void are eliminated. In the incompressible setting, it is natural to follow the same strategy. No enrichment will be used, and the weak form will be integrated in the body only.

The stability of this strategy is evaluated by considering convergence studies under total incompressibility, and numerical evaluation of the inf-sup. It will be considered as stable if the theoretical convergence rate is obtained, and if the numerical inf-sup test is passed.

4.1.1. Convergence study

Consider an infinite plate with a traction-free circular hole under uniaxial tension. The exact solution of this problem is given in [41]. We consider a square domain of edge length 2 with a circular hole of radius $a = 0.4$ at its center. The exact tractions are imposed on the boundaries of the domain and rigid body modes are prevented. The Poisson's ratio is set to 0.5 (total incompressibility), and the Young's modulus to 1.0. In addition, plane strain conditions are assumed. The sequence of meshes that we consider for the convergence study are unstructured and do not match the hole boundary (see Fig. 4a). The displacement error is measured using the energy norm error defined Eq. (22), and the error on the pressure is computed using the L^2 norm (23)

$$\varepsilon_u = \frac{\left(\int_{\Omega} (\underline{\underline{\varepsilon}}^D(u^h) - \underline{\underline{\varepsilon}}^D(u)) : \underline{\underline{\mathcal{C}}} : (\underline{\underline{\varepsilon}}^D(u^h) - \underline{\underline{\varepsilon}}^D(u)) d\Omega \right)^{1/2}}{\left(\int_{\Omega} \underline{\underline{\varepsilon}}^D(u) : \underline{\underline{\mathcal{C}}} : \underline{\underline{\varepsilon}}^D(u) d\Omega \right)^{1/2}} \quad (22)$$

$$\varepsilon_p = \frac{\left(\int_{\Omega} (p^h - p)^2 d\Omega \right)^{1/2}}{\left(\int_{\Omega} p^2 d\Omega \right)^{1/2}} \quad (23)$$

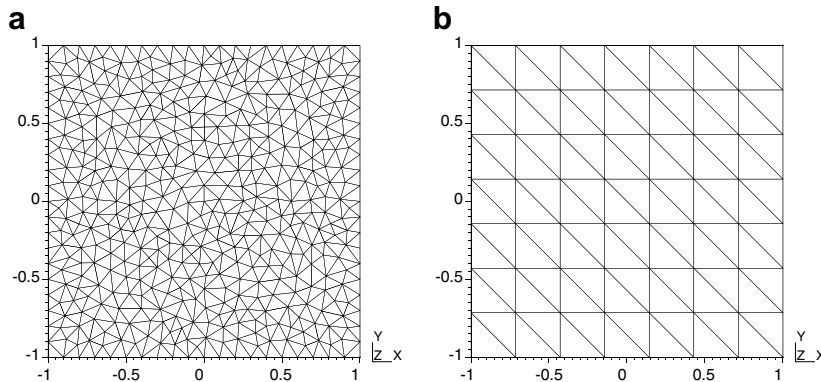


Fig. 4. (a) Sample mesh for the convergence study and (b) sample mesh for the numerical inf-sup test.

The convergence study is performed using both Mini and T6T3 elements, and the results are presented in Fig. 5 for both pressure and displacement. As seen on Fig. 5, the convergence rate of both displacement and pressure are similar to the theoretical one. This demonstrates that the X-FEM strategy for the treatment of holes preserves the convergence properties of Mini and T6T3 elements.

4.1.2. Numerical inf-sup test

Convergence study was a first step to assess the behavior of the X-FEM strategy for holes. The evaluation of the fulfilment of the inf-sup condition is another approach for the verification. We follow the work of Chapelle and Bathe [11] described in Section 2.2.2, and consider the problem presented in Fig. 6a. It is composed of a square of length 2, with a hole of radius 0.4 at its center. The square has its bottom and left edges blocked, and a pressure is applied on the upper edge. The inf-sup value is approximated using gradually refined structured triangular meshes-like the sample mesh shown in Fig. 4b. Mini and T6T3 formulations are considered herein. The evolution of the numerical inf-sup value is plotted in Fig. 6b with respect to the element size. As seen on this figure, the numerical inf-sup value is stable for both Mini and T6T3 formulations.

Remark. The resolution of the eigenvalue problem was performed using Lapack's generalized Schur decomposition routine [48].

4.2. Material inclusions

The treatment of material inclusion in a compressible media has been treated in various contributions (see for example [41,42]). In this paper, we focus on the enrichment strategy proposed by Moës et al. in [42] because this enrichment function preserves the finite element convergence rate (observed numerically), this "ridge" function is expressed as

$$\phi^u(\mathbf{x}) = \sum_{\alpha} |\zeta^{\alpha}| N^{\alpha}(\mathbf{x}) - \left| \sum_{\alpha} \zeta^{\alpha} N^{\alpha}(\mathbf{x}) \right| \quad (24)$$

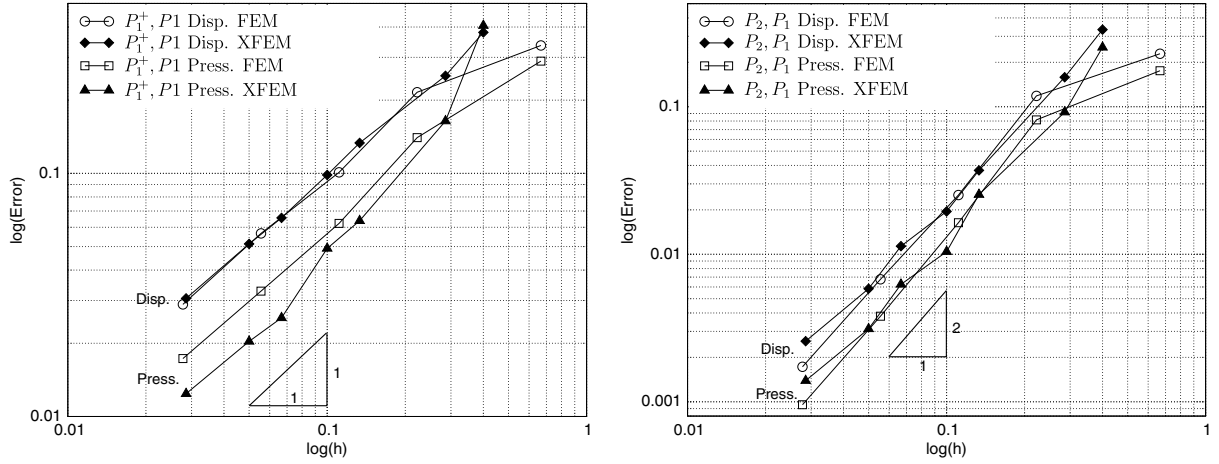


Fig. 5. Convergence study, incompressible plate with a hole. Left: Mini, right: T6T3.

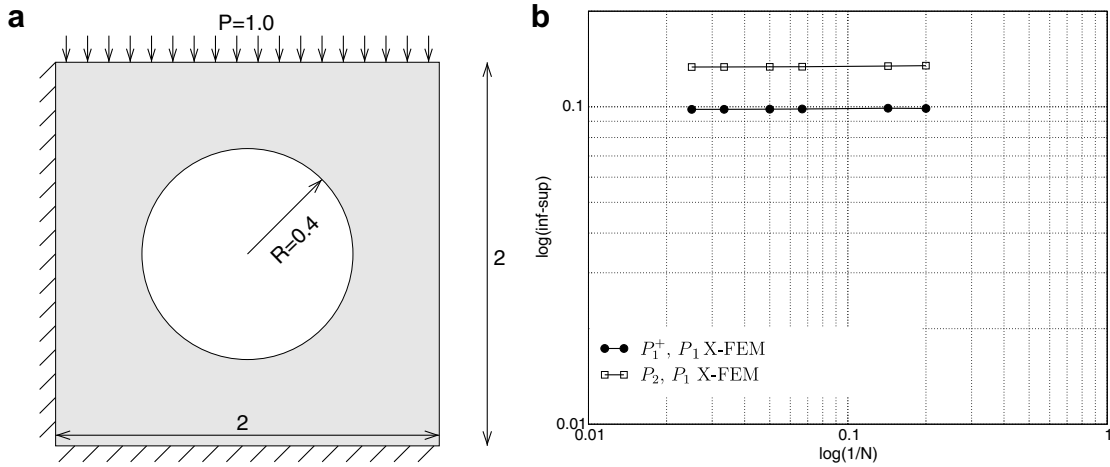


Fig. 6. Inf-sup evaluation for holes: (a) model problem and (b) evolution of the numerical inf-sup.

where ξ_i is the signed-distance function to the interface evaluated at the vertex of node i (see Fig. 7 for the example of a plate with a circular inclusion).

Two types of enrichment are considered for the pressure:

- A discontinuous enrichment (heaviside).
- A ridge function enrichment (by analogy with the strategy of enrichment of the displacement field).

Remark. Following [26], the quadrature rule is modified for the elements that are crossed by the inclusion. The partitioning of these elements and the increase in the number of Gauss points yield a sufficiently accurate integration of the weak form. More precisely, the degree of the functions to be integrated is one degree higher in the elements fully or partially enriched: the degree of the gauss integration is raised in these elements, using formulas derived by Cowper [49].

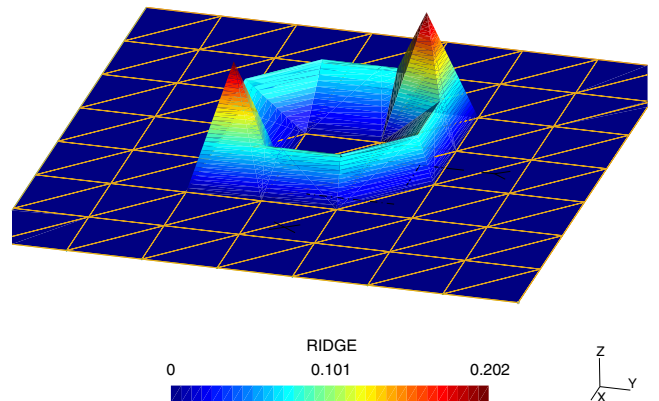


Fig. 7. Illustration of the ridge function for the case of a square plate with a circular inclusion in its center.

Table 1
Approximation spaces (R : ridge enrichment, H : heaviside enrichment)

Displacement	Pressure	Formulation no.	Convergence rate (disp./pressure)	Inf-sup test
<i>FEM-T6T3</i>				
P_2	P_1	1	$\sim 1.5^a/1.5$	PASS
<i>FEM-Mini</i>				
P_1^+	P_1	2	$\sim 1/1$	PASS
<i>X-FEM-Mini</i>				
$P_1^+ \oplus P_1^+ * R$	$P_1 \oplus P_1 * R$	3	$\sim 1/1$	PASS
$P_1^+ \oplus P_1 * R$	$P_1 \oplus P_1 * R$	4	$\sim 1/1$	PASS
$P_1^+ \oplus P_1^+ * R$	$P_1 \oplus P_1 * H$	5	$\sim 1/-^b$	PASS ^b
$P_1^+ \oplus P_1 * R$	$P_1 \oplus P_1 * H$	6	$\sim 1/-^b$	PASS ^b
<i>X-FEM-T6T3</i>				
$P_2 \oplus P_2 * R$	$P_1 \oplus P_1 * R$	7	$\sim 1.5^a/1.5$	PASS
$P_2 \oplus P_1 * R$	$P_1 \oplus P_1 * R$	8	$\sim 1.5^a/1.5$	PASS
$P_2 \oplus P_2 * R$	$P_1 \oplus P_1 * H$	9	$\sim 1.5^a/-^b$	PASS ^b
$P_2 \oplus P_1 * R$	$P_1 \oplus P_1 * H$	10	$\sim 1.5^a/-^b$	PASS ^b

^a Straight edge triangle elements.

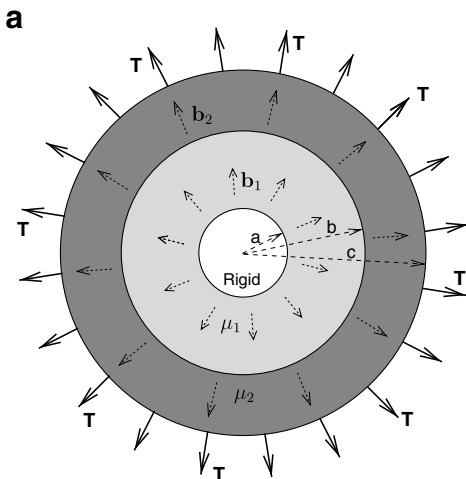
^b The inf-sup parameter is oscillatory and the pressure convergence is non-monotonous.

The stability of these enriched elements is compared to the stability of the initial ones. The finite element computation of incompressible two phase media will be handled considering Mini and T6T3 elements. The X-FEM strategies considered are presented in Table 1.

The comparison of these strategies is performed as in the previous section with convergence studies and numerical inf-sup tests.

4.2.1. Convergence studies (curved interface)

Consider the example presented in Fig. 8a. It is composed of two perfectly bounded incompressible materials with shear modulus μ_1 and μ_2 . The first material is held fixed at radius $r = a$ and the interface between the two materials is located at radius $r = b$. The structure is sub-



jected to body forces \mathbf{b}_1 and \mathbf{b}_2 in Ω_1 and Ω_2 , respectively, and tractions are enforced at radius $r = c$. The analytical pressure is depicted in Fig. 9, and detailed in Appendix A. The results of the convergence study for the mini element are presented in Fig. 10, and a typical computational mesh in shown in Fig. 8b. The energy norm error on the displacement exhibits a rate of convergence in $O(h)$ independently of the enrichment strategy. This means that concerning the displacement, the theoretical rate of convergence is preserved with all the strategies. Now, the convergence of the pressure field is considered because it is a strong indicator of the performance of a mixed formulation. Fig. 10 shows that formulations 2 and 3 give the theoretical convergence rates. Concerning formulation 5, the convergence rate is degraded when the mesh is refined. In fact, this comes from very localized pressure modes which degrade the error when the material interface crosses elements near their edges.

In Fig. 11 shows the case where only the linear part of the approximation space is enriched. As seen on this figure, the rate of convergence is also degraded for the

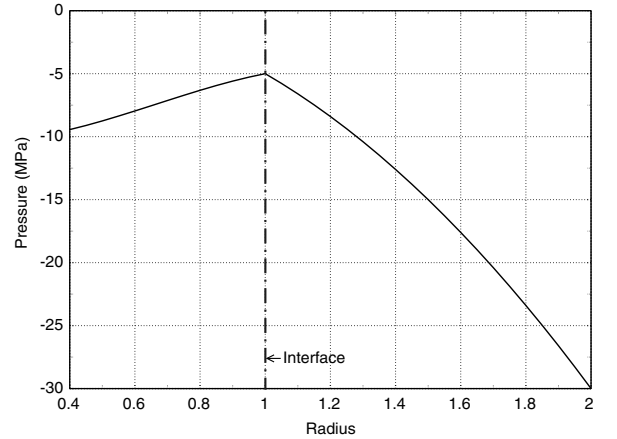


Fig. 9. Analytical pressure.

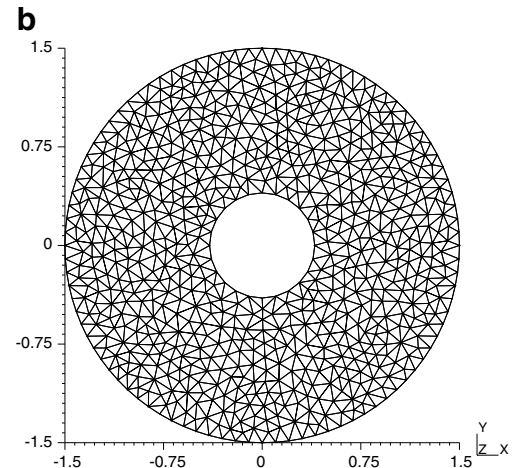


Fig. 8. (a) Shear-based example and (b) mesh used for the convergence study (note that the external radius of the mesh is smaller than c).

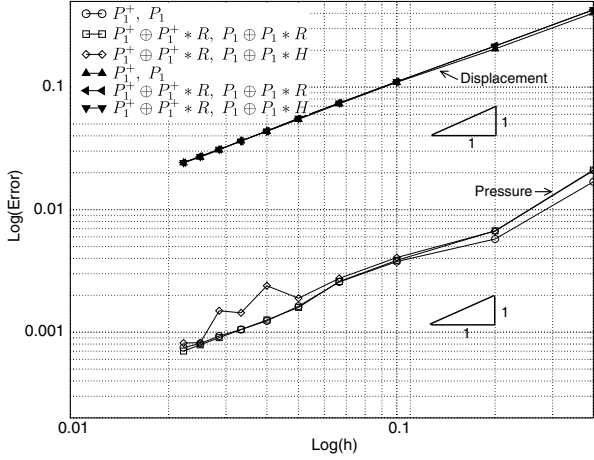


Fig. 10. Rate of convergence for the problem Fig. 8 (fully enriched mini elements).

heaviside-based enrichment when the mesh is refined. However, with ridge-based enrichment, it maintains the optimal convergence rate for both pressure and displacement.

Finally, the case of quadratic T6T3-based elements is considered in Fig. 12. The rate of convergence is $O(h^{3/2})$ for the pressure and slightly slower for the displacement (even with meshed domains). It is consistent with theory [50, p. 119]: the optimal convergence rate for curved domains discretized with triangles (straight edges) elements is $O(h^{3/2})$. The conclusions remain similar when only the linear part of the displacement is enriched (see Fig. 13). As seen in these first numerical examples, the enrichment of both pressure and displacement with the ridge function gives the theoretical convergence rates for the Mini element. In this example with T6T3 elements, the optimal rate of convergence is limited by the geometry of the problem, and not by the enrichment functions that are considered. Finally, we have seen that not enriching the bubble function gives similar results with lesser degrees of freedom. As a conclusion, it seems that the Mini element enriched

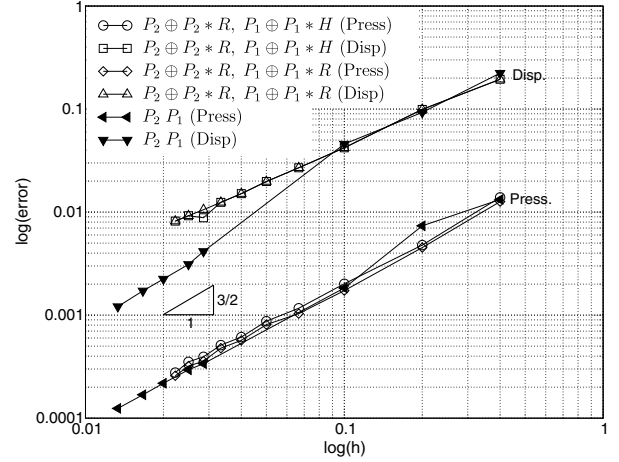


Fig. 12. Rate of convergence for the problem Fig. 8, quadratic interpolation.

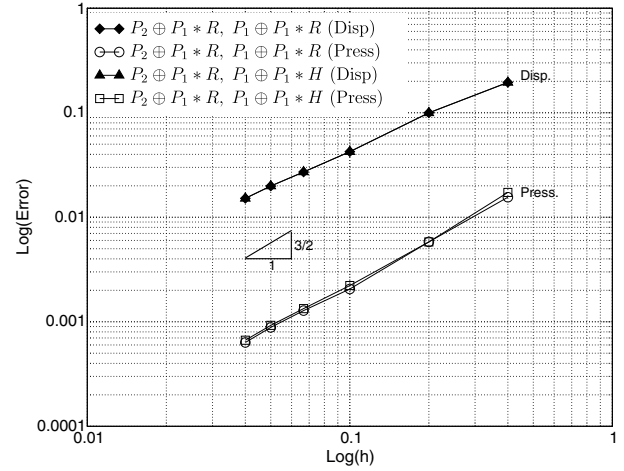


Fig. 13. Rate of convergence for the problem Fig. 8, linear part enriched (T6T3-based element).

with the ridge gives good results for total incompressibility (and thus also for almost incompressible materials).

4.2.2. Convergence studies (straight interface)

We have built another numerical example composed of a square of length 2 (see Fig. 14) which is composed of two materials 1 and 2 of shear modulus respectively μ_1 and μ_2 (the case of total incompressibility is considered). The body is subjected to surface tractions \mathbf{T} on its boundary, and body forces respectively \mathbf{b}_1 and \mathbf{b}_2 in 1 and 2. The stress, strain and pressure fields are given in Appendix B, none of them being in the finite element approximation space. Finally, we set $\mu_1 = 1/3$ and $\mu_2 = 10/3$. A convergence study is performed, and the results are given in Fig. 15. We can see that T6T3 and Mini enrichment-based strategies have the same rate of convergence than finite elements, which is optimal. This shows that ridge-based enrichment seems to have a stable behaviour in the incompressible limit.

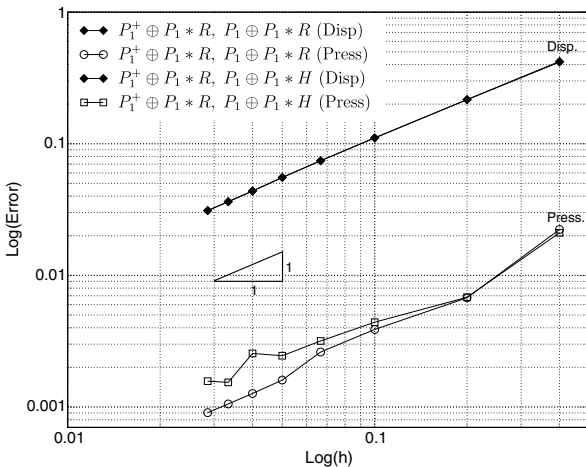


Fig. 11. Rate of convergence for the problem Fig. 8, only the linear part of the mini element is enriched.

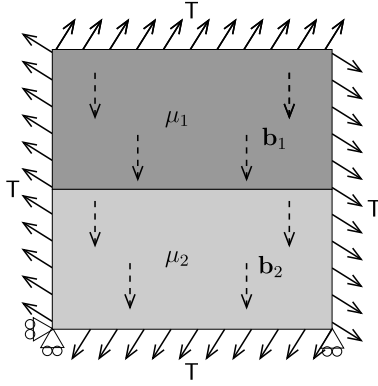


Fig. 14. Bimaterial problem with straight interface.

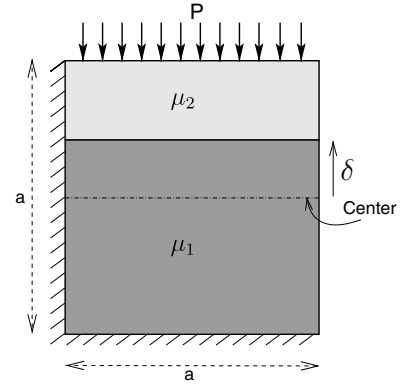


Fig. 16. Second problem for the numerical evaluation of the inf-sup.

4.2.3. Numerical inf-sup test

We have applied the numerical inf-sup test to all the examples used in the convergence study (both curved and straight interface). For the sake of simplicity, we choose here to show results of a simpler example because all the other examples present the same behaviour.

This problem, presented in Fig. 16, has been adapted from [11]. It represents a square composed of two different materials subjected to a constant pressure on its top face. The position of the interface between the two materials is parametrized by the parameter δ . First, δ is set to zero and the numerical inf-sup is evaluated. In this case, the interface is located at the center of the square and of the elements (the sequence of mesh has an odd number of elements per side). As seen in Fig. 17, the inf-sup value remains stable during refinement for all interpolation spaces.

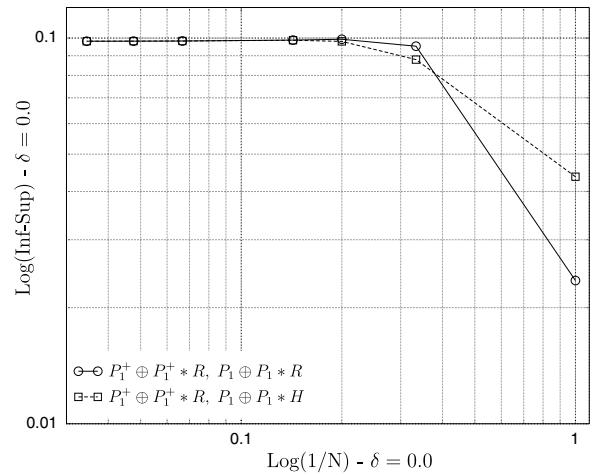


Fig. 17. Evaluation of the inf-sup ($\delta = 0.0$).

Next, δ is set to 0.1. As the interface is unsymmetrical, it will be close to the element edges at some steps of refinement. In Fig. 18, the evolution of the inf-sup parameter is now completely modified:

- For ridge-based enrichment (formulations 3 and 7), no degradation on the inf-sup is observed, the value is stable during refinement.

- Concerning the heaviside-based enrichment (formulations 5 and 9), the value of the inf-sup degrades strongly when the element edges approach the discontinuity (for $1/N \rightarrow 0.1$ or $1/N \rightarrow 0.033333$).

To study this aspect, another inf-sup test is performed with a sequence of meshes built such that the material

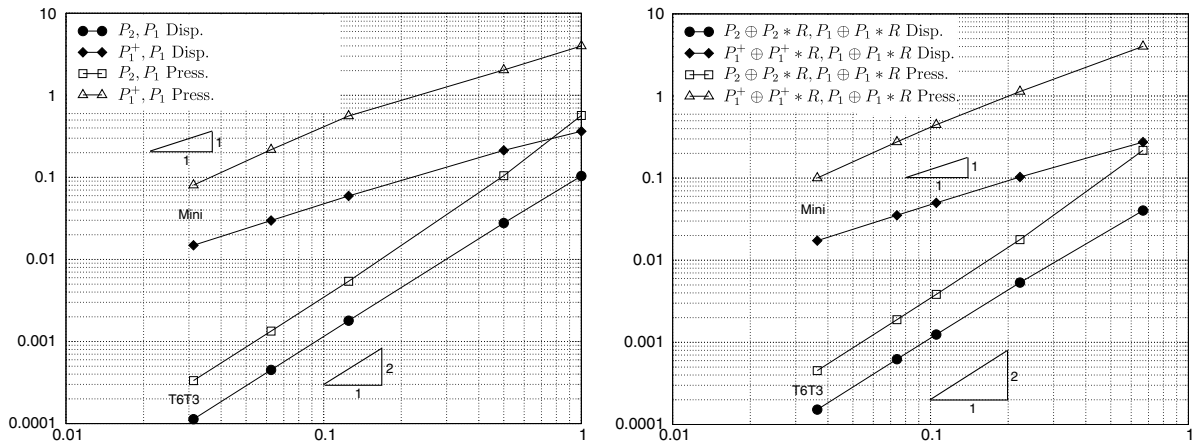


Fig. 15. Convergence study, straight interface: left, FEM; right, X-FEM.

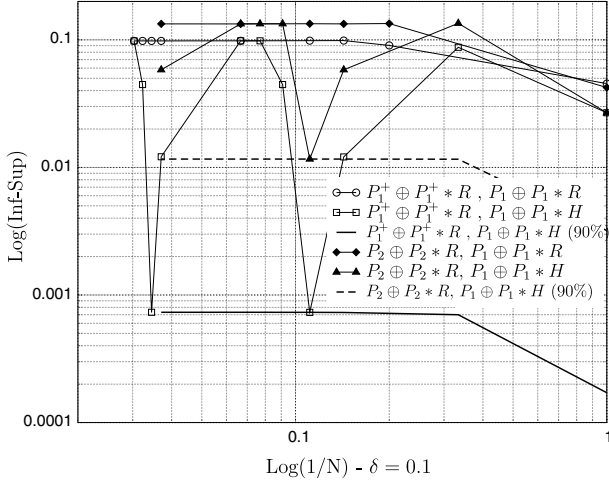


Fig. 18. Evaluation of the inf-sup ($\delta = 0.1$).

interface always crosses the elements at 90% of their height. The results correspond to the curves labeled “ $P_1^+ \oplus P_1^+ * R, P_1 \oplus P_1 * H$ (90%)” and “ $P_2 \oplus P_2 * R, P_1 \oplus P_1 * H$ (90%)” in Fig. 18.

These curves are completely stable: this means that the inf-sup condition is fulfilled even with heaviside enrichment, but that the inf-sup parameter depends on how close the material discontinuity is to the edge of the elements. This dependency does not occur for the ridge enrichment: results match the previous one. Similar results are obtained if only the linear part of the approximation space is enriched (see Fig. 19).

The dependence of the inf-sup parameter on δ and the non-monotonic convergence of heaviside-based enrichments (formulations 5 and 9) leads us to avoid these strategies to enrich the pressure.

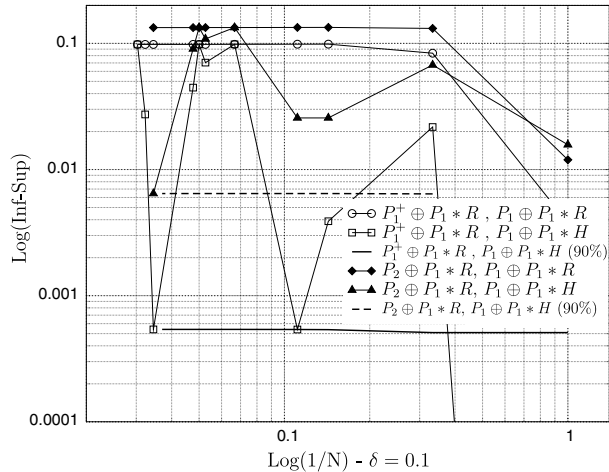


Fig. 19. Evaluation of the inf-sup (linear part enriched), problem 2 ($R = 0.1$).

4.2.4. Conclusion for material interfaces

The results presented in this section are summarized in Table 1. Strategies involving the enrichment of both displacement and pressure with the ridge function are the most effective since they pass the inf-sup test, and are not influenced by the mesh topology. On the contrary heaviside-based strategies, although satisfying the inf-sup condition, produce results which depend on the mesh topology. These strategies should not be considered. The formulations where only the linear part of the displacement is enriched (nos. 4 and 8) with the ridge are interesting, since less degrees of freedom are involved in the approximation. This should be important in the context of an extension to three dimensional studies.

Remark. The degradation of the convergence rate should be expected given the oscillations of the inf-sup parameter. This stems from the fact that the constant in the a priori error estimates depends on this parameter.

4.3. Incompressible fracture mechanics

The resolution of compressible fracture mechanics problems has been extensively studied in the context of the X-FEM for both 2D [51,26,52,40,32] and 3D fracture mechanics [29,30]. The most common enrichment strategy consists in using the asymptotic displacement field as an enrichment for the displacement finite element approximation. In the context of incompressible media, the analytical asymptotic displacement field (Westergaard solution) is shown to be identical to the limit of the compressible one. The asymptotic evolution of the pressure field can be obtained also using the Westergaard solution

$$p(r, \theta) = \frac{2K_I}{3\sqrt{2\pi r}} \cos\left(\frac{\theta}{2}\right) + \frac{2K_{II}}{3\sqrt{2\pi r}} \sin\left(\frac{\theta}{2}\right), \quad (25)$$

$$\phi^u = \left\{ \sqrt{r} \sin\left(\frac{\theta}{2}\right), \sqrt{r} \cos\left(\frac{\theta}{2}\right), \sqrt{r} \sin\left(\frac{\theta}{2}\right) \sin(\theta), \sqrt{r} \cos\left(\frac{\theta}{2}\right) \sin(\theta) \right\}. \quad (26)$$

We use these expressions as an enrichment for the pressure field in the near-tip region. Thus, the enrichment basis for the pressure is expressed as

$$\begin{cases} \phi_I^p = \frac{1}{\sqrt{r}} \cos\left(\frac{\theta}{2}\right), \\ \phi_{II}^p = \frac{1}{\sqrt{r}} \sin\left(\frac{\theta}{2}\right). \end{cases} \quad (27)$$

Note that a classical heaviside enrichment is considered for both pressure and displacement for nodes whose support is fully cut by the crack, and that only the Mini element is considered hereunder.

Remark. The elements that are crossed by the crack are partitioned, and the number of Gauss points is increased for the elements that are enriched with near-tip functions. In this case, a degenerated quadrangular Gauss quadrature is used.

4.3.1. Convergence study

Consider a domain $\Omega = [-1, 1] \times [-1, 1]$ under tension (see Fig. 20). The tensions applied on the boundary of the domain are related to the exact tensions in an infinite cracked body under mixed mode (using the Westesgaard solution with $K_I = 1.0$, $K_{II} = 1.0$). A sequence of gradually refined meshes is considered. Those meshes are built so that the crack passes always through the elements. Two types of meshes are considered: the first one is presented in Fig. 20 where the crack tip is located on an element's edge, and the second one (see Fig. 20) where it finishes inside an element. Two enrichment strategies are also considered for the near-tip region: first, the topological enrichment where only the nodes whose support contains the crack are enriched, and the so-called 'geometrical' enrichment introduced by Bechet et al. [53] where all the nodes which lie in a circle (of radius 0.1 here) are enriched with crack tip fields. The authors have shown that the convergence rate was improving from $O(h^{1/2})$ to $O(h)$ with the use of this enrichment (for a given benchmark). The convergence study are presented in Fig. 21 for the first mesh, and Fig. 22 for the second. As seen in Fig. 21, the convergence rate for both displacement and pressure are in $O(h^{1/2})$ for the topological enrichment, as expected. The influence of the enrichment is clearly drawn, as it shifts downward the displacement and pressure error curves. For a geometrical enrichment, we obtain results similar to [53], i.e. an improvement of the convergence rate up to $O(h)$ for both pressure and displacement. In this particular case, we obtain a slightly better convergence rate for the pressure. The conclusions are similar for the second mesh.

Note that the case where only the displacement field is enriched has been considered and has shown that the influence of the pressure enrichment is small when dealing with topological enrichment (changes of the initial value of the curve), whereas it is huge when dealing with the geometrical enrichment (degradation of both initial value and convergence rate). This is why, the geometrical enrichment of both pressure and displacement field is the more effective way to model incompressible fracture mechanics. Finally,

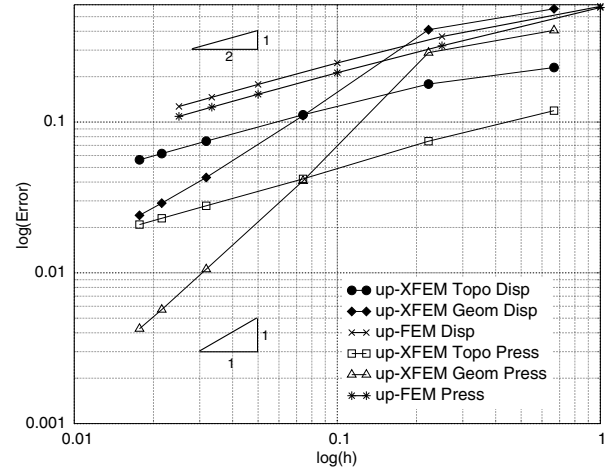


Fig. 21. Convergence rate, structured mesh no. 1.

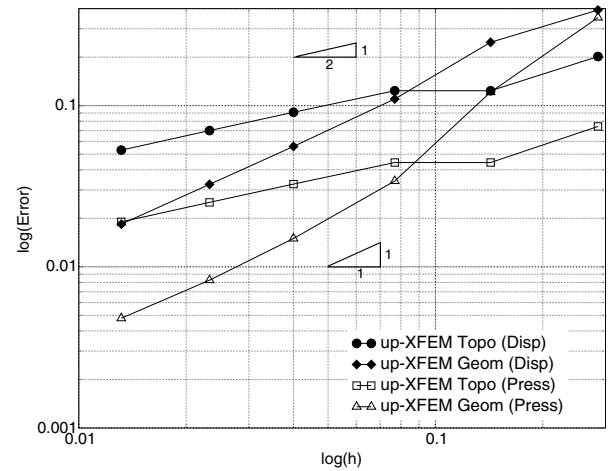


Fig. 22. Convergence rate, structured mesh no. 2.

the case where the enrichment is applied only to the linear part of the approximation is considered in Fig. 23. The rate of convergence is shown to be preserved, while degrees of freedom are saved.

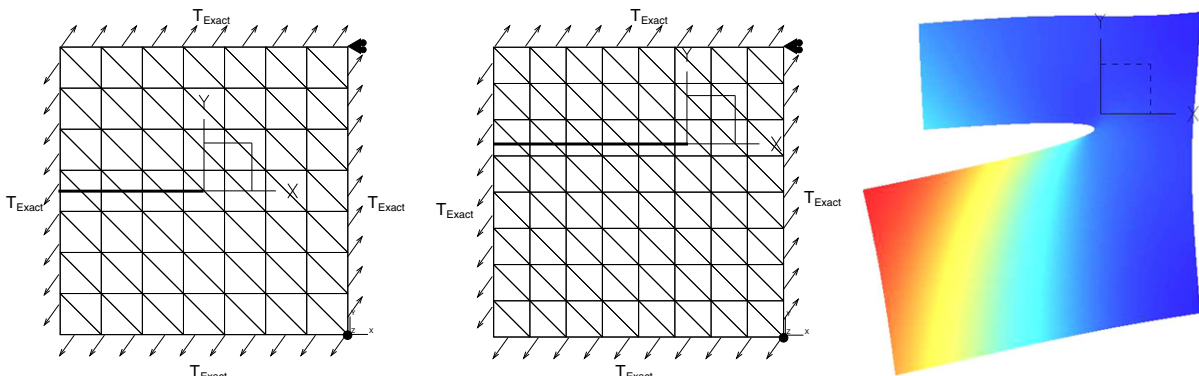


Fig. 20. Domain of interest, mesh no. 1 (left), mesh no. 2 (center) and deformed shape (right).

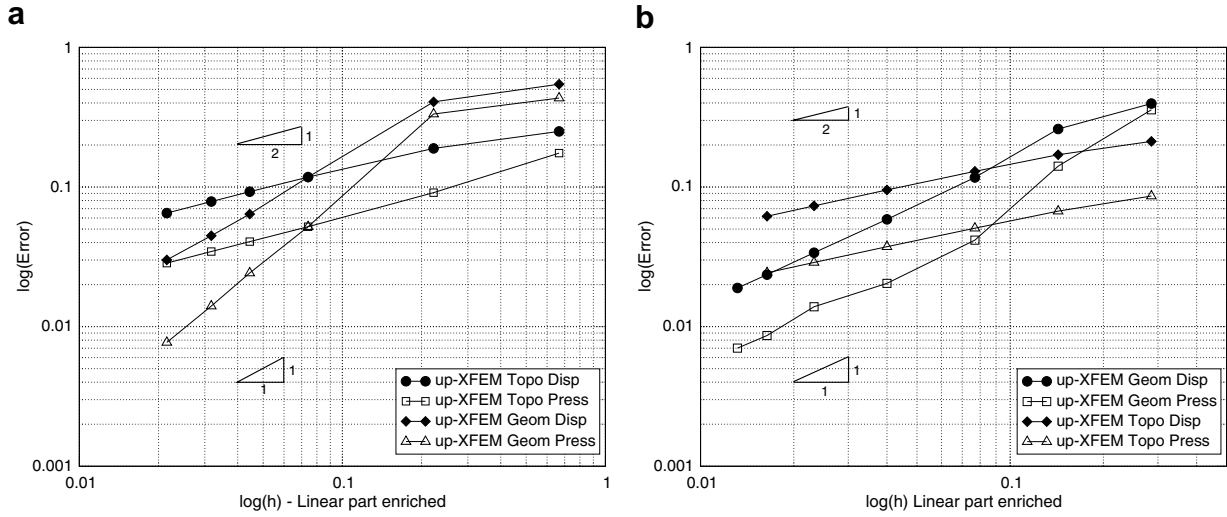


Fig. 23. Convergence rate, linear part enriched: (a) mesh no. 1 and (b) mesh no. 2.

4.3.2. Numerical inf-sup test

The evaluation of the inf-sup condition is performed by considering a single edge notched plate of side length 2.0. A pressure is applied on the upper face, bottom and left faces are held fixed. This loading case is much more drastic for the inf-sup test than the one depicted in Fig. 20. The crack tip is located at (0.1, 0.05), so that its relative position to the mesh will change during refinement (see Fig. 24). The evolution of the smallest eigenvalue of the inf-sup problem is plotted in Fig. 25 for 5 cases of figure: topological enrichment, geometrical enrichment (radius 0.4), classical FEM, topological enrichment (linear part enriched), geometrical enrichment (linear part enriched). The evolution of the eigenvalue tends to a finite value for all curves, showing that the inf-sup condition seems to be fulfilled for both of them.

4.3.3. Conclusion for fracture mechanics

We have seen that the enrichment of both displacement and pressure fields with their asymptotic expressions leads to a stable mixed formulation. Moreover, the use of the geometrical enrichment leads to an improved convergence

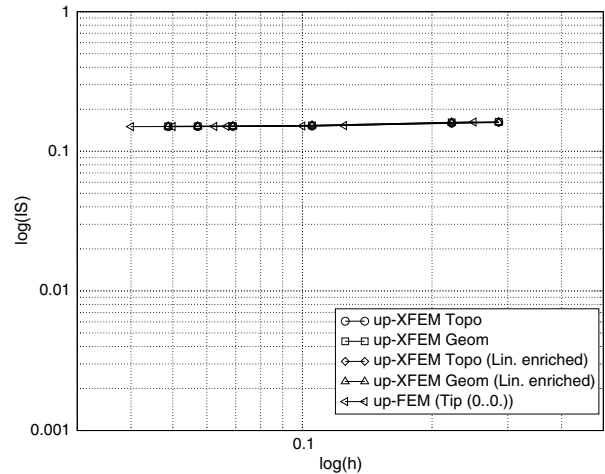


Fig. 25. Fracture inf-sup results.

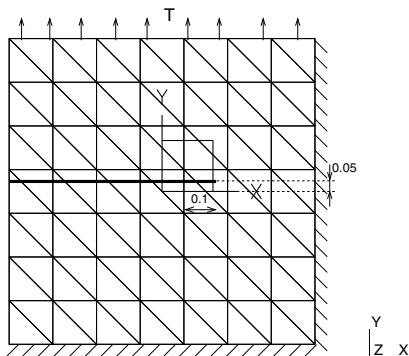


Fig. 24. Fracture inf-sup problem.

rate, similar to the compressible case. Finally, degrees of freedom can be saved by only enriching the linear part of the approximation.

5. Conclusion

Some strategies for enriching existing mixed finite element methods have been presented. These strategies are natural extensions of the displacement-based X-FEM, and are shown to preserve the classical finite element convergence rate. The stability of these strategies has been shown through the numerical inf-sup test. However, we experienced also “loss” of convergence due to curved boundaries. The construction and the validation of quadratic elements which should give back the $O(h^2)$ convergence will be the subject of a forthcoming paper. The method should also be applied to finite strain mechanics, as the fulfilment of the inf-sup condition seems to be a prerequisite to build efficient large strain formulations [54].

Appendix A. Analytical solution for curved interface

We did construct a specific analytical solution to investigate the convergence of the X-FEM. It represents two perfectly bounded rings made from different materials (see Fig. 8). The loading is chosen such that

$$b_{1r}(r) = 3W_3c^2 + 2W_2c + W_1, \quad (\text{A.1})$$

$$b_{2r}(r) = 3V_3c^2 + 2V_2c + V_1, \quad (\text{A.2})$$

$$T_r = W_3c^3 + W_2c^2 + W_1c + W_0, \quad (\text{A.3})$$

$$T_\theta = -2\frac{\mu_1\mu_2a^2b^2}{c}(-a^2\mu_1c^2 + a^2\mu_2c^2 - \mu_2b^2c^2 + a^2b^2\mu_1). \quad (\text{A.4})$$

Under these boundary conditions, the stress field components are

$$\sigma_{rr}^1 = -(W_3r^3 + W_2r^2 + W_1r + W_0), \quad (\text{A.5})$$

$$\sigma_{\theta\theta}^1 = \sigma_{rr}^1, \quad (\text{A.6})$$

$$\sigma_{r\theta}^1 = \frac{-2\mu_1\mu_2ca^2b^2}{(-a^2\mu_1c^2 + a^2\mu_2c^2 - \mu_2b^2c^2 + a^2b^2\mu_1)r^2}, \quad (\text{A.7})$$

$$\sigma_{rr}^2 = -(V_3r^3 + V_2r^2 + V_1r + V_0), \quad (\text{A.8})$$

$$\sigma_{\theta\theta}^2 = \sigma_{rr}^2, \quad (\text{A.9})$$

$$\sigma_{r\theta}^2 = \frac{-2\mu_1\mu_2ca^2b^2}{(-a^2\mu_1c^2 + a^2\mu_2c^2 - \mu_2b^2c^2 + a^2b^2\mu_1)r^2}. \quad (\text{A.10})$$

The displacement field components are

$$u_\theta^1(r) = -\frac{cb^2\mu_2(r^2 - a^2)}{(-a^2\mu_1c^2 + a^2\mu_2c^2 - \mu_2b^2c^2 + a^2b^2\mu_1)r}, \quad (\text{A.11})$$

$$u_r^1(r) = 0, \quad (\text{A.12})$$

$$u_\theta^2(r) = -c\frac{-r^2a^2\mu_2 + r^2a^2\mu_1 + r^2\mu_2b^2 - a^2b^2\mu_1}{(-a^2\mu_1c^2 + a^2\mu_2c^2 - \mu_2b^2c^2 + a^2b^2\mu_1)r}, \quad (\text{A.13})$$

$$u_r^2(r) = 0. \quad (\text{A.14})$$

And the pressure distribution is

$$p^1(r) = W_3r^3 + W_2r^2 + W_1r + W_0, \quad (\text{A.15})$$

$$p^2(r) = V_3r^3 + V_2r^2 + V_1r + V_0. \quad (\text{A.16})$$

Moreover, in the example Section 4.2.1, we have considered:

$$\mu_1 = 1/3, \quad \mu_2 = 10/3,$$

$$a = 0.4, \quad b = 1.0, \quad c = 2.0,$$

$$W_3 = -10.0, \quad W_2 = 20.0, \quad W_1 = -5.0, \quad W_0 = -10.0.$$

$$V_3 = 0.0, \quad V_2 = -10.0, \quad V_1 = 5.0, \quad V_0 = 0.0.$$

Appendix B. Analytical solution for a straight interface

The problem (see Fig. 14) is built so that the interface between the two materials is straight. The loading is chosen such that

$$b_{1x} = 6\mu_1x \quad (\text{B.1})$$

$$b_{1y} = -6\mu_1y - 2\mu_2 + 3y^2 \quad (\text{B.2})$$

$$b_{2x} = -24\mu_2x \quad (\text{B.3})$$

$$b_{2y} = 24\mu_2y - 2\mu_2 + 6y^2 \quad (\text{B.4})$$

$$T_{1x} = 6\mu_1x \quad (\text{B.5})$$

$$T_{1y} = -6\mu_1y - 2\mu_2 + 3y^2 \quad (\text{B.6})$$

$$T_{2x} = -24\mu_2x \quad (\text{B.7})$$

$$T_{2y} = 24\mu_2y - 2\mu_2 + 6y^2 \quad (\text{B.8})$$

Under these boundary conditions, the stress field components are

$$\underline{\underline{\sigma}} = \begin{pmatrix} 2\mu_1\left(-3y^2 - \frac{2\mu_2y}{\mu_1}\right) - y^3 & \mu_1\left(-\left(6y + \frac{2\mu_2}{\mu_1}\right)x + 2\right) \\ \mu_1\left(-\left(6y + \frac{2\mu_2}{\mu_1}\right)x + 2\right) & 2\mu_1\left(3y^2 + \frac{2\mu_2y}{\mu_1}\right) - y^3 \end{pmatrix}, \quad (\text{B.9})$$

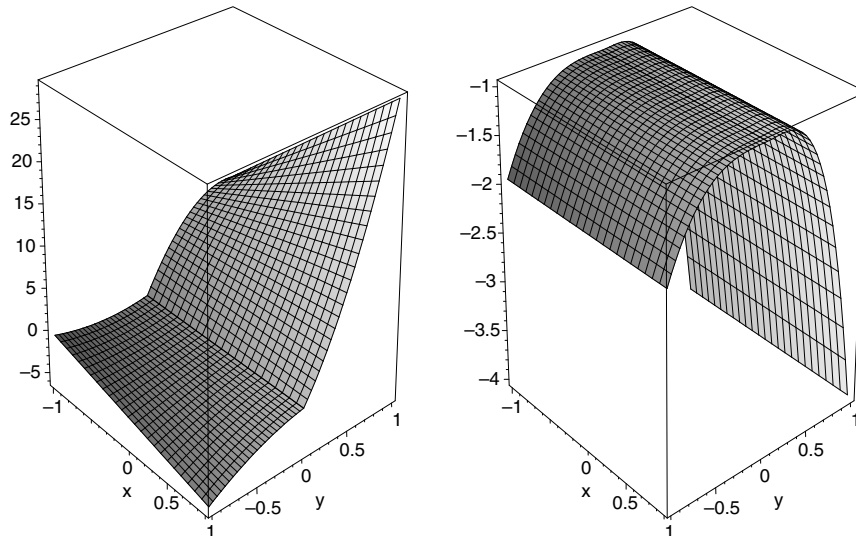


Fig. B.1. Bimaterial problem with straight interface: displacement (left: u_x , right: u_y).

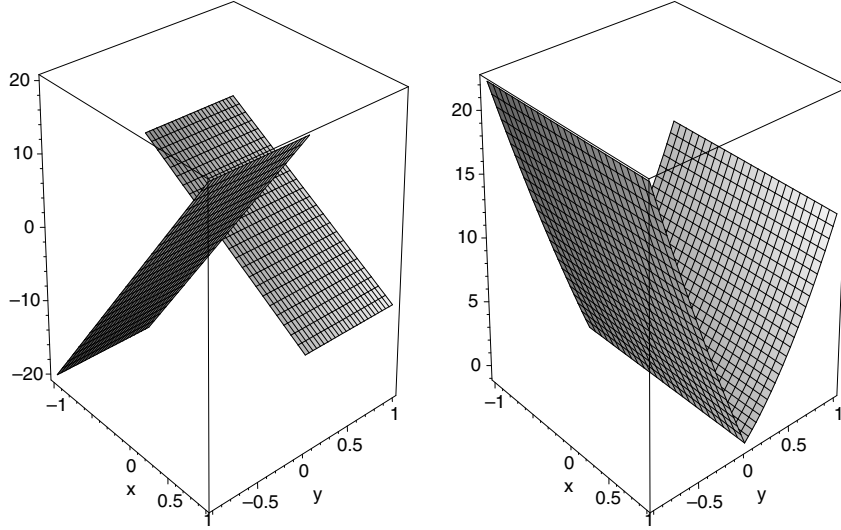


Fig. B.2. Bimaterial problem with straight interface: body forces (left: b_x , right: b_y).

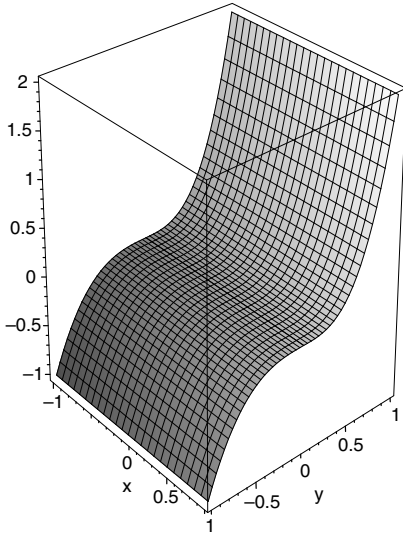


Fig. B.3. Bimaterial problem with straight interface: pressure field.

And the pressure evolution is (see Fig. B.3)

$$p_1 = y^3, \quad (\text{B.15})$$

$$p_2 = 2y^3. \quad (\text{B.16})$$

References

- [1] D.J. Naylor, Stress in nearly incompressible materials for finite elements with application to the calculation of excess pore pressure, *Int. J. Numer. Methods Engrg.* 8 (1974) 443–460.
- [2] T.J.R. Hughes, R.L. Taylor, J.F. Levy, *High Reynolds Number, Steady, Incompressible Flows by a Finite Element Method*, John Wiley & Sons, 1978.
- [3] S.F. Pawsey, R.W. Clough, Improved numerical integration of thick slab finite elements, *Int. J. Numer. Methods Engrg.* 3 (1971) 275–290.
- [4] T.J.R. Hughes, Generalization of selective reduced integration procedures to anisotropic and nonlinear media, *Int. J. Numer. Methods Engrg.* 15 (1980) 1413–1418.
- [5] R.L. Taylor, P.J. Beresford, E.L. Wilson, A nonconforming element for stress analysis, *Int. J. Numer. Methods Engrg.* 10 (6) (1976) 1211–1219.
- [6] E.L. Wilson, R.L. Taylor, W.P. Doherty, J. Ghaboussi, Incompatible displacement models, in: S.J. Fenves (Ed.), *Numerical and Computer Methods in Structural Mechanics*, Academic Press, New York, 1973, pp. 43–57.
- [7] J.C. Simo, S. Rifai, A class of mixed assumed strain methods and the method of incompatible modes, *Int. J. Numer. Methods Engrg.* 29 (1990) 1595–1638.
- [8] J.C. Simo, F. Armero, Geometrically non-linear enhanced strain mixed methods and the method of incompatible modes, *Int. J. Numer. Methods Engrg.* 33 (1992) 1413–1449.
- [9] B.D. Reddy, J.C. Simo, stability and convergence of a class of enhanced strain methods, *SIAM J. Numer. Anal.* 32 (6) (1994) 1705–1728.
- [10] F. Brezzi, M. Fortin, *Mixed and Hybrid Finite Element Methods*, Springer, New York, 1991.
- [11] D. Chapelle, K.J. Bathe, The inf-sup test, *Comput. Struct.* 47 (4–5) (1993) 537–545.
- [12] K.J. Bathe, The inf-sup condition and its evaluation for mixed finite element methods, *Comput. Struct.* 79 (2001) 243–252.
- [13] A. Huerta, S. Fernández-Méndez, Locking in the incompressible limit for the element free Galerkin method, *Int. J. Numer. Methods Engrg.* 51 (2001) 1361–1383.

$$\underline{\underline{\sigma}}_2 = \begin{pmatrix} 2\mu_2(12y^2 - 2y) - 2y^3 & \mu_2 \left(-(-24y + 2)x + 2\frac{\mu_1}{\mu_2} \right) \\ \mu_2 \left(-(-24y + 2)x + 2\frac{\mu_1}{\mu_2} \right) & 2\mu_2(-12y^2 + 2y) - 2y^3 \end{pmatrix}. \quad (\text{B.10})$$

The displacement field is (see Figs. B.1, B.2)

$$u_{1x} = - \left(3y^2 + 2\frac{\mu_2}{\mu_1}y \right) x + 2y - 1 \quad (\text{B.11})$$

$$u_{1y} = y^3 + \frac{\mu_2}{\mu_1}y^2 - 1 \quad (\text{B.12})$$

$$u_{2x} = (12y^2 - 2y)x + 2\frac{\mu_1}{\mu_2}y - 1 \quad (\text{B.13})$$

$$u_{2y} = -4y^3 + y^2 - 1 \quad (\text{B.14})$$

- [14] J. Dolbow, T. Belytschko, Volumetric locking in the element free Galerkin method, *Int. J. Numer. Methods Engrg.* 46 (6) (1999) 925–942.
- [15] A. Huerta, Y. Vidal, P. Villon, Pseudo-divergence-free element free Galerkin method for incompressible fluid flow, *Comput. Methods Appl. Mech. Engrg.* 193 (12–14) (2004) 1119–1136.
- [16] A. Huerta, S. Fernández-Méndez, Enrichment and coupling of the finite element and meshless methods, *Int. J. Numer. Methods Engrg.* 48 (11) (2000) 1615–1636.
- [17] J.M. Melenk, I. Babuška, The partition of unity finite element method: basic theory and applications, *Comput. Methods Appl. Mech. Engrg.* 139 (1996) 289–314.
- [18] C.A. Duarte, J.T. Oden, An h - p adaptive method using clouds, *Comput. Methods Appl. Mech. Engrg.* 139 (1–4) (1996) 237–262.
- [19] C. Duarte, J. Oden, An hp meshless, in: *Method Numerical Methods for Partial Differential Equations*, vol. 12, 1996, pp. 673–705.
- [20] T. Strouboulis, I. Babuška, K. Copps, The design and analysis of the generalized finite element method, *Comput. Methods Appl. Mech. Engrg.* 181 (2000) 43–69.
- [21] T. Strouboulis, K. Copps, I. Babuška, The generalized finite element method, *Comput. Methods Appl. Mech. Engrg.* 190 (32–33) (2001) 4081–4193.
- [22] C.A. Duarte, I. Babuška, J.T. Oden, Generalized finite element methods for three-dimensional structural mechanics problems, *Comput. Struct.* 77 (2) (2000) 215–232.
- [23] J.T. Oden, C.A.M. Duarte, O.C. Zienkiewicz, A new cloud-based hp finite element method, *Commun. Numer. Methods Engrg.* 153 (1–2) (1998) 117–126.
- [24] T. Strouboulis, L. Zhang, I. Babuška, Generalized finite element method using mesh-based handbooks: application to problems in domains with many voids, *Comput. Methods Appl. Mech. Engrg.* 192 (2003) 3109–3161.
- [25] T. Strouboulis, L. Zhang, I. Babuška, p -version of the generalized FEM using mesh-based handbooks with applications to multi-scale problems, *Int. J. Numer. Methods Engrg.* 60 (10) (2004) 1639–1672.
- [26] N. Moës, J. Dolbow, T. Belytschko, A finite element method for crack growth without remeshing, *Int. J. Numer. Methods Engrg.* 46 (1999) 131–150.
- [27] N. Sukumar, Z.Y. Huang, J.H. Prévost, Z. Suo, Partition of unity enrichment for bimaterial interfacial cracks, *Int. J. Numer. Methods Engrg.* 59 (2004) 1075–1102.
- [28] E. Budyn, G. Zi, N. Moës, T. Belytschko, A model for multiple crack growth in brittle materials without remeshing, *Int. J. Numer. Methods Engrg.* (2004).
- [29] N. Moës, A. Gravouil, T. Belytschko, Non-planar 3D crack growth by the extended finite element and level sets. Part I: mechanical model, *Int. J. Numer. Methods Engrg.* 53 (2002) 2549–2568.
- [30] A. Gravouil, N. Moës, T. Belytschko, Non-planar 3D crack growth by the extended finite element and level sets. Part II: level set update, *Int. J. Numer. Methods Engrg.* 53 (2002) 2569–2586.
- [31] N. Sukumar, N. Moës, T. Belytschko, B. Moran, Extended finite element method for three-dimensional crack modelling, *Int. J. Numer. Methods Engrg.* 48 (11) (2000) 1549–1570.
- [32] J. Dolbow, N. Moës, T. Belytschko, An extended finite element method for modeling crack growth with frictional contact, *Comput. Methods Appl. Mech. Engrg.* 190 (2001) 6825–6846.
- [33] J. Dolbow, N. Moës, T. Belytschko, Modeling fracture in Mindlin–Reissner plates with the extended finite element method, *Int. J. Solids Struct.* 37 (2000) 7161–7183.
- [34] N. Moës, T. Belytschko, Extended finite element method for cohesive crack growth, *Engrg. Fract. Mech.* 69 (2002) 813–834.
- [35] G.N. Wells, L.J. Sluys, A new method for modelling cohesive cracks using finite elements, *Int. J. Numer. Methods Engrg.* 50 (2001) 2667–2682.
- [36] J. Réthoré, A. Gravouil, A. Combescure, An energy-conserving scheme for dynamic crack growth using the extended finite element method, *Int. J. Numer. Methods Engrg.* 53 (2005) 2569–2586.
- [37] J.E. Dolbow, A. Devan, Enrichment of enhanced assumed strain approximations for representing strong discontinuities: addressing volumetric incompressibility and the discontinuous patch test, *Int. J. Numer. Methods Engrg.* 59 (2004) 47–67.
- [38] G. Legrain, N. Moës, E. Verron, Stress analysis around crack tips in finite strain problems using the extended finite element method, *Int. J. Numer. Methods Engrg.* 63 (2005) 290–314.
- [39] P.M.A. Areias, T. Belytschko, Analysis of three-dimensional crack initiation and propagation using the extended finite element method, *Int. J. Numer. Methods Engrg.* 63 (5) (2005) 760–788.
- [40] C. Daux, N. Moës, J. Dolbow, N. Sukumar, T. Belytschko, Arbitrary branched and intersecting cracks with the extended finite element method, *Int. J. Numer. Methods Engrg.* 48 (2000) 1741–1760.
- [41] N. Sukumar, D.L. Chopp, N. Moës, T. Belytschko, Modeling holes and inclusions by level sets in the extended finite element method, *Comput. Methods Appl. Mech. Engrg.* 190 (2001) 6183–6200.
- [42] N. Moës, M. Cloirec, P. Cartraud, J.-F. Remacle, A computational approach to handle complex microstructure geometries, *Comput. Methods Appl. Mech. Engrg.* 192 (2003) 3163–3177.
- [43] J. Chessa, T. Belytschko, An extended finite element method for two-phase fluids, *J. Appl. Mech.* 70 (1) (2003) 10–17.
- [44] G.J. Wagner, N. Moës, W.K. Liu, T. Belytschko, The extended finite element method for stokes flow past rigid cylinders, *Int. J. Numer. Methods Engrg.* 51 (2001) 293–313.
- [45] D.S. Malkus, Eigenproblems associated with the discrete LBB condition for incompressible finite elements, *Int. J. Engrg. Sci.* 139 (10) (1981) 1299–1310.
- [46] D.N. Arnold, F. Brezzi, M. Fortin, Stable finite element for stokes equations, *Calcolo* 21 (1984) 337–344.
- [47] O.C. Zienkiewicz, Y.C. Liu, G.C. Huang, Error estimates and convergence rates for various incompressible elements, *Int. J. Numer. Methods Engrg.* 28 (1989) 2191–2202.
- [48] LAPACK Linear Algebra PACKage. <<http://www.netlib.org/lapack/>>.
- [49] G.R. Cowper, Gaussian quadrature formulas for triangles, *Int. J. Numer. Methods Engrg.* 7 (1973) 405–408.
- [50] Pierre Arnaud Raviart, Jean-Marie Thomas, *Introduction à l’analyse numérique des équations aux dérivées partielles*, Dunod, Paris, 1998.
- [51] T. Belytschko, T. Black, Elastic crack growth in finite elements with minimal remeshing, *Int. J. Numer. Methods Engrg.* 45 (5) (1999) 601–620.
- [52] D.L. Chopp, N. Sukumar, Fatigue crack propagation of multiple coplanar cracks with the coupled extended finite element/fast marching method, *Int. J. Engrg. Sci.* 41 (2003) 845–869.
- [53] E. Béchet, H. Minnebo, N. Moës, B. Burgardt, Improved implementation and robustness study of the X-FEM for stress analysis around cracks, *Int. J. Numer. Methods Engrg.* 64 (8) (2005) 1033–1056.
- [54] D. Pantuso, K.J. Bathe, On the stability of mixed finite elements in large strain analysis of incompressible solids, *Finite Elem. Anal. Des.* 28 (1997) 83–104.